Dalton Transactions

PAPER

View Article Online
View Journal | View Issue

Cite this: *Dalton Trans.*, 2015, **44**, 3454

Modulation of electronic and redox properties in phenolate-rich cobalt(III) complexes and their implications for catalytic proton reduction†

Debashis Basu, Marco M. Allard,‡ Fernando R. Xavier,§ Mary Jane Heeg, H. Bernhard Schlegel and Claudio N. Verani*

Received 31st October 2014,
Accepted 2nd January 2015

DOI: 10.1039/c4dt03337j

www.rsc.org/dalton

We investigate the redox, spectroscopy and catalytic reactivity of new cobalt(III) complexes based on phenolate-rich [N_2O_3] ligands. These complexes are described as [$Co^{III}(L^X)$MeOH], where X indicates the presence of chloro (**1**), bromo (**2**), iodo (**3**), or *tert*-butyl (**4**) substituents in the 3rd and 5th positions of each phenolate ring. These substituents modulate the Co(III) ← $PheO^-$ LMCT bands of the parent complexes with **1** (451) > **2** (453) > **3** (456) > **4** (468 nm) and the redox potentials involved with the Co(III)/Co(II) and ligand reduction and with the phenolate/phenoxyl oxidation processes. The influence of the substituents on the phenolate pendant arms was also observed on the kinetic parameters; **1** presented a rate constant of 1.0×10^{-3} s^{-1} whereas **4** showed a considerably slower rate (5.3×10^{-5} s^{-1}). Species **1** and **4** are electrocatalysts towards proton reduction in the presence of weak acid in acetonitrile. A TON of 10.8 was observed for **1** after 3 h of bulk electrolysis at −2.20 V_{Fc/Fc^+} using a mercury pool as the working electrode.

Introduction

Considering the impending limitations of fossil fuels and the increasing demand for energy, the search for earth-abundant catalysts capable of hydrogen production is at the core of an economy based on renewable fuels.[1] The cobalt ion has been used in several proton-reduction electrocatalysts because of its energetically viable conversion from $3d^6$ ^{LS}Co(III) or $3d^7$ Co(II) into the procatalytic nucleophile $3d^8$ ^{LS}Co(I) species.[2] This state captures a proton to yield a reactive Co(III)H species which, pending on specific conditions can stay as Co(III)H or undergo reduction to generate a related Co(II)H; These hydride species are able to react with another proton, thus yielding H_2.[3] Several ligands have been studied to accommodate the cobalt ion; chief designs include oximes, pending-arm polypyridines, macrocycles, and iminopyridines.[4] Although phenolate-based cobalt complexes have been used in olefin and epoxide polymerization,[5] these complexes are less studied for proton reduction because of the expected high overpotentials associated with the Co(II)/Co(I) couple, but the search for new architectures that either yield new catalysts or allow for rationalizations about catalyst design[6] is impending.

Our group is engaged in the chemistry of cobalt complexes with redox-active phenolate-rich environments focusing on tridentate [NN′O][7] and pentadentate [N_2O_3][8] ligands to predict structural, electronic and redox properties of metallosurfactants, and the reactivity of metallodrugs. In [N_2O_3] environments with three *t*-butyl-decorated phenolates[8] four reversible redox-accessible states are present; three involving distinct phenolato/phenoxyl radical couples between 0.3 and 1.0 $V_{Fc^+/Fc}$ and one process associated with the Co(III)/Co(II) couple at −0.6 $V_{Fc^+/Fc}$. The redox processes were cycled 30 times without major decomposition at the surface of the electrode. These results are encouraging because reversibility of redox processes along with modulation of the Co(III)/Co(II) potential may be relevant for the development of proton reduction catalysts.

With the previous arguments in mind, we hypothesize that the nature of phenolate-linked substituent will modulate the potential by which cobalt(III)/(II) reduction takes place. In this article we investigate the structural, electronic and redox behavior of four complexes, shown in Scheme 1, by means of experimental and computational methods. We also evaluate their behavior as electron acceptors in ascorbic acid-mediated reductions and in proton reduction in acidic media. The results follow.

Department of Chemistry, Wayne State University, Detroit, MI 48202, USA.
E-mail: cnverani@chem.wayne.edu; Fax: +313577 8022; Tel: +313 577 1076

†Electronic supplementary information (ESI) available. CCDC 1012180 and 1012179. For ESI and crystallographic data in CIF or other electronic format see DOI: 10.1039/c4dt03337j

‡Current address: Department of Chemistry, La Sierra University, Riverside, CA 92515, USA.

§Current address: Department of Chemistry, Santa Catarina State University, Joinville 89219, Brazil.

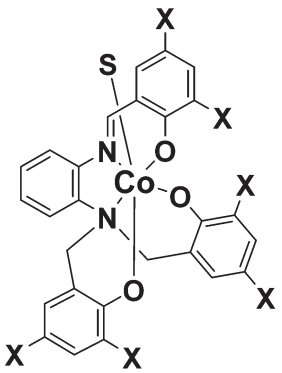

X = Cl; S = MeOH (1)
X = Br; S = MeOH (2)
X = I; S = MeOH (3)
X = *t*-Bu; S = MeOH (4)

Scheme 1 Cobalt(III) complexes.

Results and discussion

Syntheses and characterizations

A series of asymmetrical pentadentate ligands was synthesized by treatment of 1,2-diaminobenzene with 2,4-disubstituted-chloromethylphenol precursors bearing chloro (**1**), bromo (**2**), iodo (**3**) and *t*-butyl (**4**) functionalities in presence of triethylamine in dichloromethane (Fig. S1†). Pale yellow solids were obtained for each ligand after brine extraction and characterized with spectroscopic (FTIR and ^{1}H-NMR) and ESI-MS spectrometric methods. The ligands were dissolved in methanol and treated with cobalt(II) perchlorate under aerobic conditions and in the presence of sodium methoxide to afford the desired cobalt(III) complexes **1–4** (Fig. S2†). During the course of the reaction, the cobalt(II) ion is oxidized into cobalt(III) and the ligand is oxidized from its amine to the imine form. This amine/imine conversion has been observed in iron complexes with related ligands.[9]

Compounds **1–4** were characterized by spectroscopic and spectrometric methods. The FTIR spectra for each complex confirms a C=N stretching around 1585 cm^{-1} resulting from ligand oxidation. The absence of peaks associated with the perchlorate anions confirms **1–4** as neutral Co(III) species, in excellent agreement with the resulting elemental analyses. High-resolution ESI mass spectra show the species $[M + H^+]^+$, $[M + Li^+]^+$, and $[M + Li^+]^+$, for **1–3**, respectively (Fig. S3†). Experimental and simulated isotopic distributions are in agreement with the proposed molecular composition. Due to the diamagnetic nature of the low spin cobalt(III) complexes the ^{1}H-NMR spectra for all the complexes were taken in d^6-DMSO. The spectra have shown appropriate line-splitting patterns for **1–4** with 10 typical aromatic protons, the azomethine proton resonance (over the aromatic region) and four methylene hydrogens between 4.0 and 5.0 ppm. A methanol molecule bound to the sixth coordination position of the Co(III) center was assigned with a resonance line between 3.0 and 3.3 ppm for **1–4**. Species **4** shows intense peaks between 0 to 2 ppm due to the presence of *tert*-butyl substituents. Selected ^{1}H-NMR spectra for **1** and **4** are shown in Fig. 1 while the spectra for **2** and **3** are shown in the ESI as Fig. S4 and S5.† Species **1**, and **2** had their molecular structures solved by X-ray analysis, while complex **4** was described previously.[8]

Molecular structures

Complexes **1**, and **2** yielded well-formed brown crystals used for single crystal X-ray diffractometric analysis. The atomic labeling schemes of **1**, and **2** are shown in Fig. 2 while selected bond lengths and angles are shown in Table 1.

Complexes **1** and **2** belong to a *C*2/*c* monoclinic space group. Both crystal structures reveal a mononuclear $[Co^{III}L^X(MeOH)]$ neutral complex unit (X = Cl or Br) where each of the cobalt(III) centers is in an $[N_2O_4]$ coordination environment. A distorted octahedral geometry is imposed over the metallic ion by the three phenolate arms, the rigid azomethine, the amine moieties, and the coordinated methanol molecule, as summarized by the selected bond lengths and angles shown in Table 1. In all three structures the O1 oxygen atoms associated with the iminophenolates are coordinated to the Co1 center in a *trans* position to the N2 amine nitrogen atom, while the O2 and O3 aminophenolate oxygen atoms are *trans* to each other. The O4 oxygen atom of the weakly bound protonated molecule of methanol is *trans* to the N1 imine nitrogen atoms. This Co–O(4) is the longest, reaching 1.95 to 2.01 Å. The Co–$O_{phenolate}$ bonds vary between 1.87 and 1.92 Å, with the Co–O2 bonds being slightly longer than Co–O1 and Co–O3. The Co–N bonds show considerable length variability, with a short Co-N1 ≈ 1.87 Å associated with the C=N group (N1–C7 ≈ 1.29 Å) and longer Co–N2 ≈ 1.98 Å associated with the amine group. The average N1–C8 bond length at 1.41 Å for **1** and **2** is slightly shorter than the equivalent N2–C13 (av. 1.47 Å), thus suggesting electron delocalization along with the 1,2-diaminobenzene ring and the iminophenolate arm (Fig. S6†). Shorter O1–C1 (av. 1.30 Å) and C6–C7 (av. 1.42 Å) bonds reinforce the argument while the C6–C7–N1–C8 dihedral angles of 177.7(3)° for **1** and 174.3(8)° for **2** reveal planarity indicative of a conjugated π framework. The geometrical arrangement, as well as the bond lengths and angles are isostructural with the previously reported **4** and other species in similar $[N_2O_3O_{MeOH}]$ environments.[8]

Electronic and electrochemical properties

Calculated electronic structures. Insight into the nature of the molecular orbitals of complexes **1**, **2**, and **4** were obtained by means of DFT calculations. Complexes **4** were modeled replacing the *t*-butyl groups of the phenolate rings by methyl groups ($\mathbf{4^{Me}}$). In agreement with the ^{1}H-NMR data, the orbital occupancies are shown in Fig. 3 plotted as comparative molecular orbital ladders of diamagnetic closed shell singlets of 3d^6 ^{LS}Co(III) complexes. The calculated bond lengths are consistent with the experimental values determined by X-ray diffraction with differences between 0.002–0.043 Å, well within acceptable range. An energy difference of 0.6 eV (~14 kcal

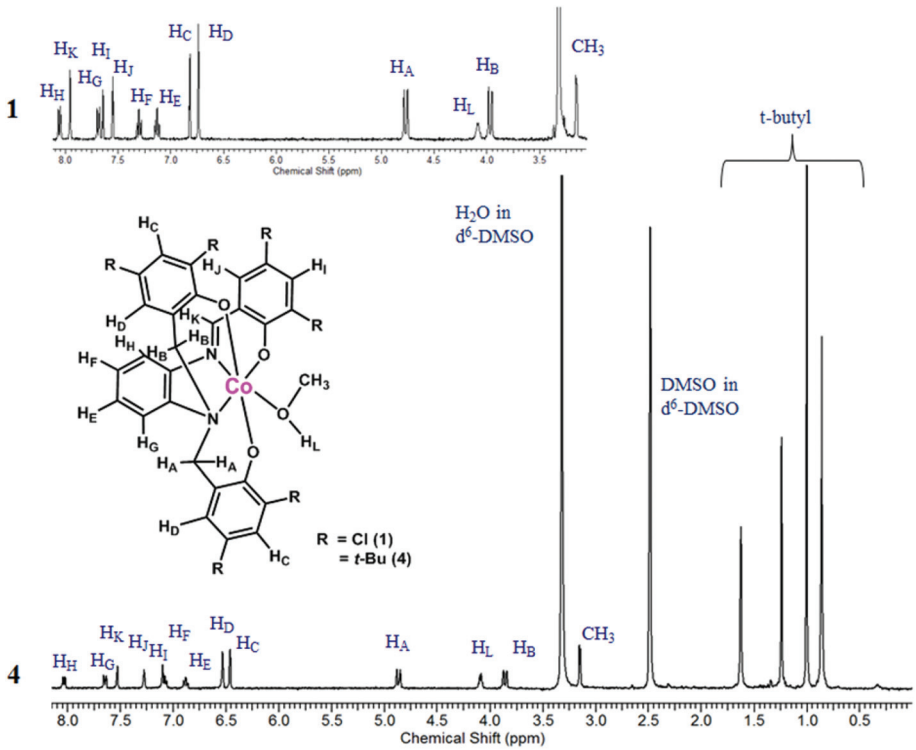

Fig. 1 ^{1}H-NMR spectra for compounds **1** and **4** in d^{6}-DMSO.

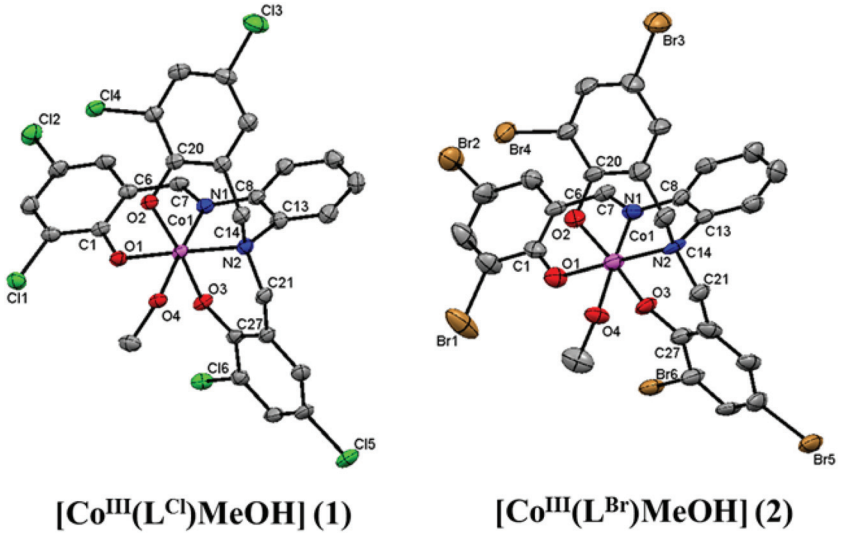

Fig. 2 ORTEP[10] representations of **1**, and **2** (left to right).

mol^{-1}) becomes evident, when comparing the highest occupied molecular orbitals (HOMOs) of the electron-withdrawing chloro-substituted **1** with those of the electron-donating methyl-substituted **4**. The first four HOMOs, namely HOMO, HOMO−1, HOMO−2, and HOMO−3 are predominantly based on the phenolato groups, in good agreement with previous assignments.[7d,e,8,11,12] Species **1**, **2**, and **4** are comparable to each other in MO occupancy and orbitals energies (Fig. 3 and Fig. S7†). A noticeable effect of halogen substitution on **1** and **2** is the energy lowering of the first three unoccupied orbitals LUMO, LUMO+1, and LUMO+2 which correspond to the empty π* orbital of the imine, and two empty Co-based orbitals respectively.

Effect of ligand substitution and solvents in the electronic spectra. The electronic spectra of **1**–**4** were measured in acetonitrile and dichloromethane (Fig. 4 and S8†) and summarized in Table 2. UV-visible spectra were also measured in other coordinating solvents (Fig. S9†). The complexes show charge-

Table 1 Selected bond lengths and bond angles

1	2
Co1–N1···1.878(2)	Co1–N1···1.879(8)
Co1–N2···1.986(2)	Co1–N2···1.981(8)
Co1–O1···1.871(2)	Co1–O1···1.886(7)
Co1–O2···1.9077(19)	Co1–O2···1.925(7)
Co1–O3···1.8834(19)	Co1–O3···1.870(7)
Co1–O4···1.9627(19)	Co1–O4···1.955(7)
N1–C7···1.296(4)	N1–C7···1.305(12)
N2–C14···1.517(4)	N2–C14···1.520(13)
N2–C21···1.498(4)	N2–C21···1.501(11)
N1–C8··· 1.426(4)	N1–C8···1.406(12)
N2–C13···1.470(3)	N2–C13 1.473(14)
O1–C1···1.297(3)	O1–C1···1.302(12)
O2–C20···1.331(3)	O2–C20···1.357(11)
O3–C27···1.316(3)	O3–C27···1.336(10)
N1–Co1–O2···92.88(9)	N1–Co1–O2···92.6(3)
O1–Co1–O2···85.41(9)	O1–Co1–O2···86.3(3)
O2–Co1–O4···87.93(8)	O2–Co1–O4···89.4(3)
O2–Co1–N2···94.81(9)	O2–Co1–N2···93.4(3)
O1–Co1–N1···96.04(10)	O1–Co1–N1···95.4(3)
O1–Co1–O3···87.58(9)	O1–Co1–O3···88.4(3)
O1–Co1–O4···87.27(8)	O1–Co1–O4···86.5(3)
N1–Co1–N2···85.65(10)	N1–Co1–N2···85.7(3)
N1–Co1–O3···87.65(9)	N1–Co1–O3···87.8(3)
O3–Co1–N2···92.21(9)	O3–Co1–N2···91.9(3)
O4–Co1–N2·····91.03(9)	O4–Co1–N2···92.5(3)
O3–Co1–O4···91.95(8)	O3–Co1–O4···90.5(3)

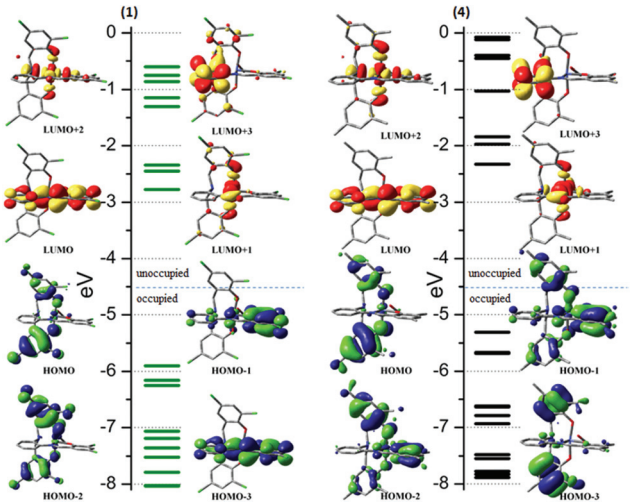

Fig. 3 MO ladders and plots for **1** (left) and **4** (right).

transfer absorptions between 400 and 800 nm along with processes below 400 nm, typically associated with ligand-centered charge transfer.

The two strong but ill-solved bands between 400–500 nm are attributed to a phenolate-to-azomethine intraligand charge transfer (ILCT, 450–475 nm) and a ligand-to-metal charge transfer process (LMCT) involving an in-plane $p\pi_{phenolate} \rightarrow d\sigma^*_{Co(III)}$ transition[13] (475–500 nm). The shoulders seen at lower energy (550–800 nm) are attributed to out-of-plane $p\pi_{phenolate} \rightarrow d\sigma^*_{Co(III)}$[14] LMCT processes. A modest variation in the position of the ILCT and in-plane LMCT processes can be associated with the electron withdrawing or donating nature of

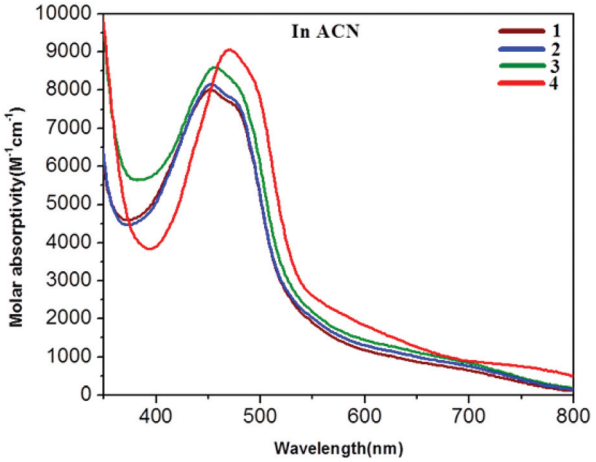

Fig. 4 UV-Visible spectra of **1–4** (1.0×10^{-4} M; acetonitrile).

Table 2 UV-Visible spectroscopic data for **1–4** in dichloromethane and acetonitrile

Compound	λ_{max}, nm/(ε, M^{-1} cm^{-1}) in acetonitrile	λ_{max}, nm/(ε, M^{-1} cm^{-1}) in dichloromethane
1	451 (8034), 475 (7602), 697 (594)	455 (7431), 486 (7323), 712 (565)
2	453 (8160), 476 (7751), 696 (755)	456 (8077), 486 (7782), 712 (582)
3	456 (8592), 479 (8053), 697 (796)	457 (8684), 487 (8012), 712 (634)
4	468 (9011), 492 (8305), 757 (656)	471 (8798), 496 (8174), 759 (958)

the phenolate-installed substituents in the order **1** < **2** < **3** < **4**. Similarly, the LMCT bands for **1–3** in acetonitrile are hypsochromically shifted by 8–16 nm, when compared to dichloromethane, thus indicating that acetonitrile replaces the weakly bound methanol molecule in solution. Although changes are more subtle for **4**, the ability to replace methanol is relevant for proton-reduction catalysis.

Time-dependent DFT methods were used to model and assign the bands observed in acetonitrile spectra of **1**, and **4** (Fig. 5 and S10†); The simulated spectrum of **1** indicates a lower energy band at 683 nm associated with an aminophenolate-to-Co(III) CT and in good agreement with the experimentally observed band at 697 nm. The main CT contribution at higher energy originates from amino/iminophenolate-to-phenyleneimine and amino/iminophenolate-to-Co(III) (Table S1†). Two distinct bands result from multiple processes calculated between 390–520 nm; one at *ca.* 430 nm and another at 500 nm. Both bands are in relatively good agreement with the experimentally observed processes at 451 and 475 nm and are relevant to indicate the origin of the experimental CT processes. Calculated TD-DFT spectra for **4** also show similar behavior (Fig. S10 and Tables S2†).

Effect of ligand substituents on the redox behavior. Cyclic voltammograms (CV) for **1**, **2**, and **4** were recorded in aceto-

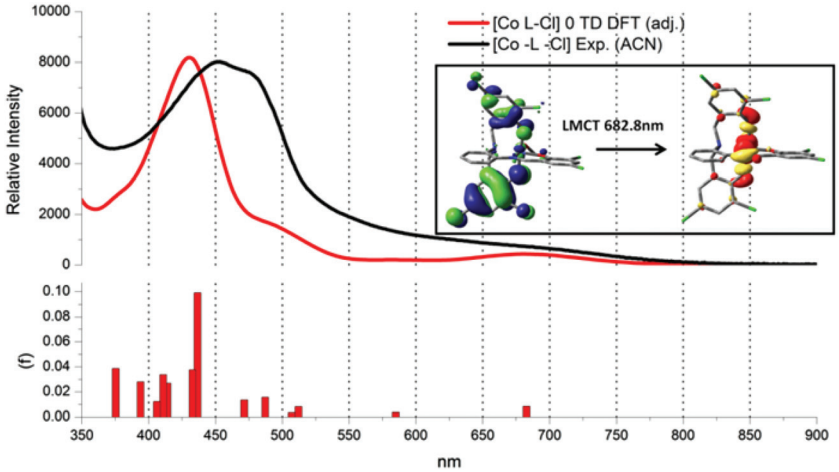

Fig. 5 Absorption spectra for **1** in CH_3CN.TD-DFT calculated spectra (red trace) in CH_3CN as solvent model and experimental spectra (black trace) in the same solvent. The inset indicates the lowest energy transition.

Table 3 Cyclic voltammetric data for **1–4** in CH_3CN

	3^{rd} $PhO^-/PhO^{\bullet}$ $E_{1/2}$, V (ΔE, V) $\lvert i_{pc}/i_{pa}\rvert$	2^{nd} $PhO^-/PhO^{\bullet}$ $E_{1/2}$, V (ΔE, V) $\lvert i_{pc}/i_{pa}\rvert$	1^{st} $PhO^-/PhO^{\bullet}$ $E_{1/2}$, V (ΔE, V) $\lvert i_{pc}/i_{pa}\rvert$	Co(III)/Co(II) $E_{1/2}$, [E_{pc}; E_{pa}], V (ΔE, V) $\lvert i_{pc}/i_{pa}\rvert$	C=N/C$^{\bullet}$–N$^-$ $E_{1/2}$, V (ΔE, V) $\lvert i_{pc}/i_{pa}\rvert$
1	+1.33 (0.13) |0.82|	+1.09 (0.08) |0.95|	+0.73 (0.08) |1.00|	−0.63 [−0.72; −0.52] (~0.20) |1.7| Spike at E_{pa} = −0.15	−2.03 (0.06) |1.43|
2	+1.33 (0.05)	+1.06 (0.09) |0.53|	+0.70 (0.08) |0.30|	−0.68 [−0.80; −0.56] (0.22) |1.8|	−2.06 (0.11) |7.29| −2.20 (0.09) |2.53|
3[a]	—	—	—	Spike at E_{pa} = −0.16	E_{pc} = −2.07; E_{pc} = −2.25
4	+0.99 (0.16) |0.82|	+0.58 (0.07) |0.98|	+0.21 (0.07) |0.97|	−0.64 [−0.72; −0.56] (0.12) |1.06|	−2.55 (0.08) |1.09|

[a] **3** in DMF.

nitrile using $TBAPF_6$ (0.1 M) as supporting electrolyte. Compound **3** was measured in *N*,*N*′-dimethylformamide due to solubility restrictions. Potentials were measured against Ag/AgCl and are reported *versus* the Fc/Fc^+ redox couple. Table 3 summarizes the electrochemical data and Fig. 6 (**1** and **4**) and Fig. S11 and S12† (**2** and **3**) display the results. Voltammograms taken in dichloromethane for **1** and **4** are displayed in Fig. S13† and data tabulated in Table S3,† show comparable behaviors to those in acetonitrile (Fig. S13†).

Compound **1** (Fig. 6, top) shows three reversible phenolate/phenoxyl processes between 0.50 and 1.50 V_{Fc/Fc^+} while a reversible process at −2.03 V_{Fc/Fc^+} is attributed to the reduction of the phenylene-imine moiety.[15] The process attributed to the cobalt(III)/(II) couple is quasi-reversible with E_{pc} and E_{pa} respectively at −0.72 and *ca.* −0.52 V_{Fc/Fc^+}, corresponding to an $E_{1/2} \approx -0.63$ V_{Fc/Fc^+} with $|i_{pc}/i_{pa}| = 1.7$.[7d,16] This process is obfuscated by a sharp spike at −0.15 V_{Fc/Fc^+} associated to an unidentified product. Compound **2**, (Fig. S11†) shows a less reversible profile with three phenolate/phenoxyl processes between 0.70 and 1.50 V_{Fc/Fc^+}, whereas the phenylene-imine process is split in two irreversible waves between −1.80 and −2.50 V. As the phenylene-imine moiety can accept 2 electrons, we infer that two electrons are transferred at slightly different potentials. We did not pursue this issue. The metal-centered process was quasi-reversible with E_{pc} = −0.80 and E_{pa} = −0.56 V_{Fc/Fc^+} and $E_{1/2} \approx -0.68$ V_{Fc/Fc^+}. The CV for **3** was taken in DMF is shown in Fig. S12† over a narrower voltage window in the anodic region that prevents further discussion of the phenolate/phenoxyl processes. An irreversible cobalt(III)/(II) reduction was observed at $E_{pc} = -1.04$ V_{Fc/Fc^+}, along with two irreversible processes attributed to the phenylene-imine observed with E_{pc} values of −2.07 and −2.25 V_{Fc/Fc^+}. Complex **4** (Fig. 6, middle) showed three reversible phenolate/phenoxyl processes between 0.10 and 1.25 V_{Fc/Fc^+} and one reversible phenylene-imine process at −2.55 V_{Fc/Fc^+}. Additionally—contrary to the barely reversible behavior observed for **1–3**—the Co(III)/Co(II) redox couple observed at −0.64 V_{Fc/Fc^+} exhibited excellent reversibility with ΔE = 0.12 and $|i_{pc}/i_{pa}| = 1.06$.

The quasi-reversible behavior observed for **1–3** is associated with the reorganizational energy barrier for the Co(II)/Co(III) couple.[17] The E_{pc} values for the Co(III)/(II) couple in **1** and **4** vary by ~0.72 V, whereas the imine based process (2^{nd} reduction) shifted to more negative potentials by 0.5 V. This variation is attributed to electronic effects of the different

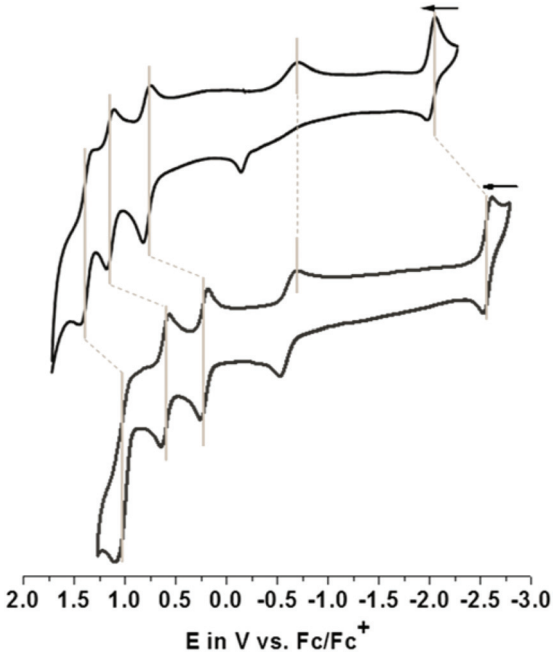

Fig. 6 Cyclic Voltammograms of **1** (top), and **4** (bottom) in acetonitrile. Conditions: 0.1 M $TBAPF_6$ as supporting electrolyte; Glassy carbon (working), Pt wire (counter) and Ag/AgCl (reference); Scan rate: 100 mV s^{-1}.

substituents attached to the imino-phenolate rings, and the more electronegative the substituent, the less electron density will be centered in the imine unit, resulting in less negative reduction potentials. For **1**—containing electron-withdrawing –Cl substituents—the lowest reduction potential for the imine process is observed. For the oxidative couples, the electrochemical potentials for the phenolates shifted to less positive values when substitution changes from the more electron-withdrawing chloro to the more donating *tert*-butyl group. Higher electron density upon the phenolate rings facilitates electrochemical oxidation and so, potentials tend to be less positive with a ~0.5 V_{Fc/Fc^+} shift from **1** to **4**. The potentials of **1–4** were recorded 5 times using different stock solutions to confirm reproducibility of the data.

Redox potentials were calculated *via* DFT methods and showed comparable values to the experimental data (Table S4 and Fig. S14†). In order to confirm the redox loci observed, we have evaluated the frontier molecular orbitals (MOs) for selected systems. These MOs are directly related to the reactivity of complexes and have proven useful in comparing the relevant redox sequences between species **1** and **4**. In order to make calculations more affordable, we modeled the *tert*-butyl substituents in **4** using methyl groups. All five electrochemical processes were probed and are summarized in Fig. 7. Spin density plots resulting from reduction, namely $[CoL]^-$, $[CoL]^{2-}$, as well as oxidation, namely [CoL], $[CoL]^+$ $[CoL]^{2+}$ and $[CoL]^{3+}$ were obtained. Interestingly, the second phenolate-based oxidation, $[CoL]^{2+}$, occurs at the amino-phenolate moiety for the $\mathbf{4}^{\mathbf{CH_3}}$, whereas for the chloro-substituted **1** this oxidation originates from the imino-phenolate (Fig. S15,† 7). An observed extended conjugation for **1** and other halogeno-substituted complexes is most likely the reason behind this phenomenon.

The first reduction yields spin density on the cobalt center, consistent with a high spin Co(II) while the second reduction is solely based on the imine moiety with most of the added electron being shared between the carbon and nitrogen atoms. Upon the addition of this second electron, we observed a significant bond length increase of 0.06 Å in the C=N bond. This is consistent with our previous assignment of this reduction as exclusively ligand-based. As reduction processes are relevant for proton reduction catalysis, usual attributions include the transformations Co(III) → Co(II) → Co(I). For species **1–4** we did not observe the Co(II)/Co(I) couple, instead we observed a ligand-based reduction that follows the Co(III)/Co(II) couple.

Better understanding of the redox processes observed for **1–4** was achieved *via* spectropotentiostatic experiments in acetonitrile (or dimethylformamide for **3**) using $TBAPF_6$ as supporting electrolyte. When the potential was fixed in −1.40 V_{Fc/Fc^+} spectral changes in the visible region were observed as shown in Fig. 8. The LMCT absorption bands between 450 and 800 nm decrease, in agreement with the proposed Co(III)/Co(II) redox pair. Isosbestic points were observed at *ca.* 430–440 nm reflecting a decrease in the LMCT bands at 475–500 nm, while new absorption bands appeared at 420–440 nm for all complexes. The disappearance of the LMCT bands upon reduction suggests these new bands do not require the involvement of the metal center, thus supporting the TD-DFT assignment of intraligand charge transfer ($\pi_{phenolate} \rightarrow \pi^*_{imine}$).

When a fixed potential was applied at −2.40 V_{Fc/Fc^+} (for **1–3**) targeting the azomethine process, the initial response within *ca.* 10 min was similar to that shown in Fig. 8a. However after the full reduction of the cobalt(III) center, the ILCT absorption

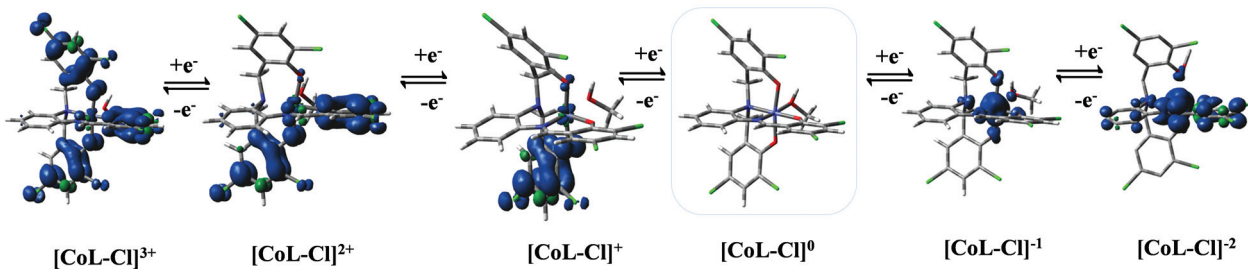

Fig. 7 Spin density plots for redox processes in **1**.

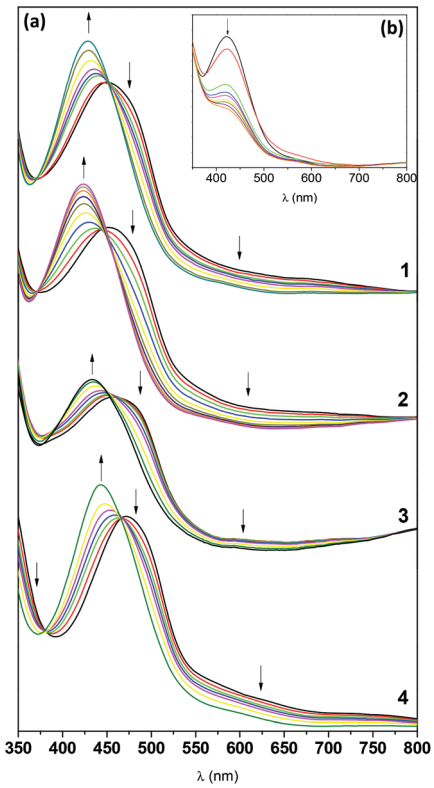

Fig. 8 (a) Spectral changes upon electrochemical reduction of the Co(III)/Co(II) process in **1**, **2** and **4** in acetonitrile and **3** in DMF. The applied potential was −1.40 V_{Fc/Fc^+} over a period of 10 min; (b) Spectral changes upon second reduction of **1** in acetonitrile. The applied potential was −2.40 V_{Fc/Fc^+} and the graph represents the behavior after 10 min. $TBAPF_6$ (0.1 M) was used as supporting electrolyte.

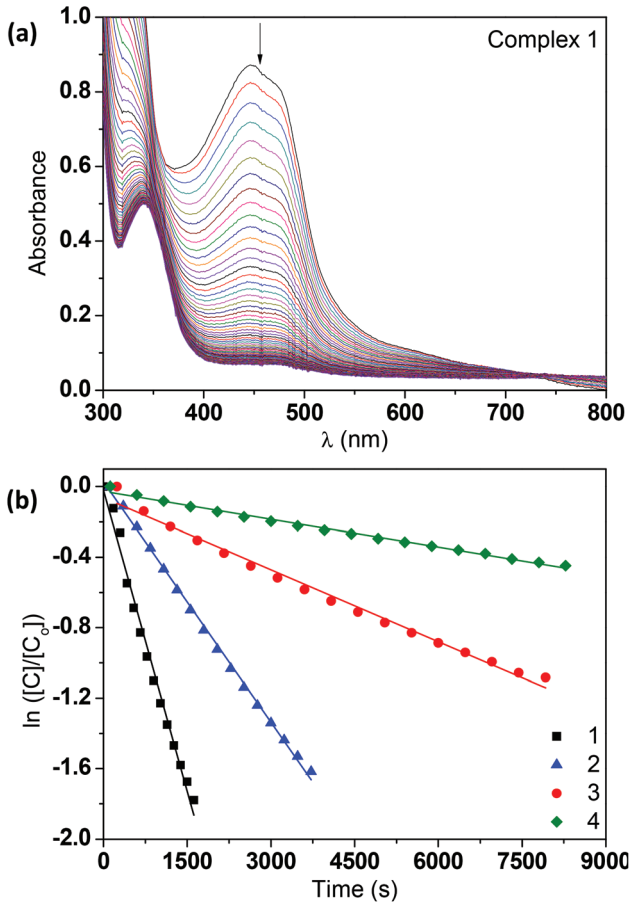

Fig. 9 (a) Time-dependent UV-Visible spectral changes in acetonitrile–water (90 : 10% v/v) for complex **1**; (b) Chemical reduction tests for **1–4** with the reducing agent ascorbic acid. Conditions: $[C]_{final}$ = 1.80 × 10^{-4} M, [AA] = 2.00 × 10^{-2} M and pH ~ 3.0.

gradually starts to decrease (Fig. 8b and Fig. S16†). This is indicative that the azomethine moiety becomes reduced. As for oxidations, when the potential was fixed to 0.85 V_{Fc/Fc^+} for **1–3** (and 0.30 V_{Fc/Fc^+} for **4**) a band appeared around 1000 nm, which has been ascribed to a phenolate to phenoxyl ILCT process[12,18] (Fig. S17†). This is in good agreement with our previous observations in similar systems.[8] TD-DFT calculations were used to model the experimentally observed changes in the visible spectrum of **1**, both upon cobalt(III) reduction and phenolate oxidation. The first reduction results in disappearance of the LMCT process whereas the ILCT band remains intact. Similarly, oxidation results in a peak around 600–800 nm, along with another band at very low energy (~1500 nm). Both observations are in excellent agreement with the experimental findings (Fig. 8, S18 and S19†).

Reactivity studies

Behavior as electron acceptors. As phenolates stabilize the trivalent cobalt in complexes **1–4**, conversion of Co(III) into Co(II) is a fundamental step relevant for catalysis. In order to understand the electron acceptance ability of **1–4**, chemical reduction tests were carried out using excess ascorbic acid as the reductant. Opposite to an electrochemical reduction, in which slow and sometimes incomplete redox processes take place due to the timescale of the experiment, chemical reductions tend to be faster and more complete. Spontaneous electron transfer reaction from ascorbic acid to **1–4** is assured by the electrochemical potentials observed for the Co(III)/Co(II) couple,[19] and the experiments were performed in CH_3CN–H_2O (90 : 10% v/v). Results were evaluated spectrophotometrically following the disappearance of the phenolate-to-cobalt(III) LMCT processes in the parent compounds at room temperature (Fig. 9a, Fig. S20†). This disappearance is due to the conversion of the low-spin $3d^6$ Co(III) into a $3d^7$ Co(II) species that precludes the Co(III) ← PhO^- LMCT process. Plots of complex concentrations *vs.* time were obtained and fitted using a first order exponential decaying equation (Fig. S21†) and linearized using a first order rate equation (Fig. 9b). From the linearized data, the rate constants (k_{obs}) and half-life values ($t_{1/2}$) were obtained for the complexes **1–4** and are listed in Table 4.

The electronic influence of the substituents present on the phenolate pendant arms was clearly observed on the kinetic parameters. Compound **1** presented a rate constant of 1.0 × 10^{-3} s^{-1} whereas compound **4** showed a considerably slower rate of 5.3 × 10^{-5} s^{-1}. Based on these results we conclude that the rate constants (k_{obs}) tend to decrease when electron-with-

Table 4 Kinetic parameters obtained for the chemical reduction reaction between complexes **1–4** and ascorbic acid[a]

	Complexes			
Parameter	**1**	**2**	**3**	**4**
k_{obs} (s^{-1})	1.0×10^{-3}	4.4×10^{-4}	1.3×10^{-4}	5.3×10^{-5}
$t_{1/2}$ (min)	12	26	89	220

[a] Acetonitrile–water (90 : 10% v/v); $[C]_{final} = 1.80 \times 10^{-4}$ M, [AA] = 2.00×10^{-2} M, pH ~ 3.0 at room temperature.

drawing groups such as chloro are replaced by electron-donating groups such as ^{t}butyl. Half-lives ($t_{1/2}$) for **1–4** were also calculated. For these electron transfer reactions, the $t_{1/2}$ values follow the same trend observed for the rate constants. The results show clearly the time-wise efficiency of the complex **1**, where in 12 minutes 50% of that species had been reduced to its Co(II) counterpart. For complex **4**, on the other hand, the $t_{\frac{1}{2}}$ value is approximately 20-fold lower. This behavior can be explained in terms of electron density over the metallic center: electron deficiency is triggered on the metal when electron-withdrawing groups are present, making the cobalt(III) centers more positive and electron acceptance easier. Overall, the trend can be summarized as follows: 1 (–Cl) > 2 (–Br) > 3 (–I) > 4 (^{t}Bu).

Behavior as proton-reduction catalysts. We tested the activity of compounds **1–4** towards proton reduction in presence of a weak acid such as acetic acid (HOAc). We focused our attention on complexes **1** and **4** due to their inherently different redox and electronic natures. These species show their catalytic wave in close vicinity to the ligand-based imine process (Fig. 10a and Fig. S22†). Overpotential was calculated to be 0.60 V and 0.90 V for **1** and **4**, respectively. Species **1** generated H_2 at lower overpotentials than those observed for the *t*-butyl substituted **4**. This is tentatively associated with the presence of the electron-withdrawing chloro substituents. Comparison of the cyclic voltammogram between **1** and a control blank was also performed. The blank contained ten equivalent of acetic acid in absence of the catalyst. The system containing **1** generated dihydrogen at a lower overpotential of 0.35 V when compared to the blank (Fig. 10b and Fig. S23†). Hydrogen generation was confirmed from bulk-electrolysis measurements for **1** at an applied potential of −2.20 V_{Fc/Fc^+}, and an associated turnover number (TON) of 10.8 was determined after three hours with a faradaic efficiency of 85% using a Hg-pool as working electrode, Ag/AgCl as the reference electrode, and a platinum wire as the auxiliary electrode. Charge consumption over time is observed to be considerably higher when the cobalt complex is present (Fig. 10c), thus validating species **1** as a viable catalyst. Furthermore, the catalyst generates 660 μmol of hydrogen in three hours of bulk-electrolysis at −2.2 V_{Fc/Fc^+}. This is a 16 fold increase in comparison to a negligible 40 μmol of hydrogen observed for the control under identical conditions. Each set of experiments was repeated in triplicate using fresh solutions. During the controlled potential

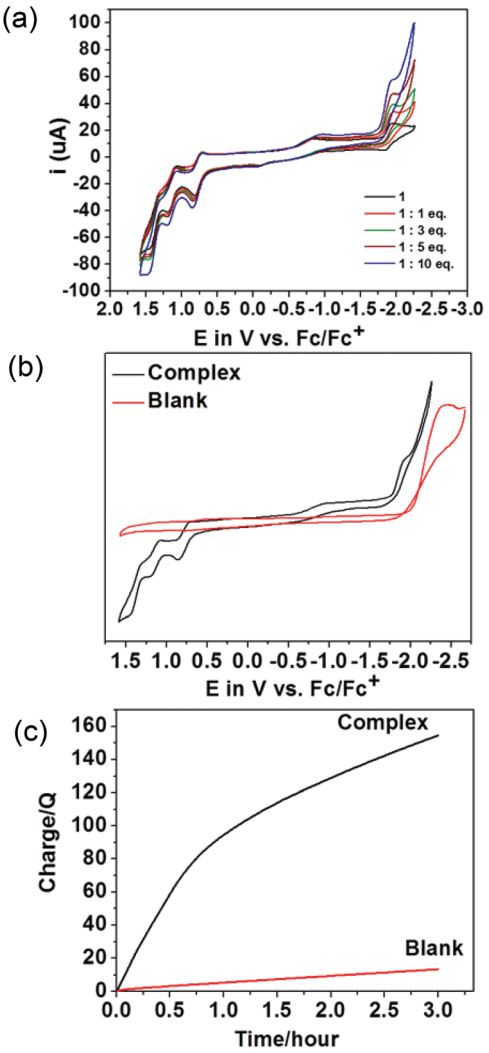

Fig. 10 (a) Electrocatalytic activity of complex **1** towards proton reduction in presence of acetic acid. (b) Comparison of cyclic voltammogram between **1** and blank in the presence of 10 equivalents of acetic acid. [Conditions for (a) and (b): Glassy carbon (WE); Pt-wire (AE); Ag/AgCl (RE)]. (c) Charge *vs.* time plot over 3 h during bulk-electrolysis at −2.2 V_{Fc/Fc^+} of **1** in comparison to the blank. [Conditions: Hg-pool (WE); Pt-coil (AE); Ag/AgCl (RE)].

experiment, no deposition of any solids was observed on the electrode surface. Moreover, analysis of the post-catalysis solution suggested the presence of a Co^{II}-species within a similar ligand environment, as shown by the UV-Visible spectra (Fig. S24†). The attribution of the spectral profile is based on similarities with that of the Co(II) spectra obtained during spectroelectrochemistry. Similar bulk-electrolysis measurements were not possible for **4** due to its high overpotential. Appearance of the catalytic peak close to the imine-based process suggested the doubly reduced state as the catalytic species. On the other hand, protonation of the phenolates in these conditions was ruled out due to unchanged UV-Visible spectra for either **1** or **4** upon addition of much stronger nitric acid to acetonitrile.

Fig. S23† shows a comparison of the redox-catalytic data to the blank sample and confirms lower overpotential and higher increase of current in presence of the complexes. This behavior validates the complexes as the catalysts. Species **1** displays chloro-substituted phenolates accepted to withdraw electronic density from the metal center, thus turning the metal ion more electrophilic and helping stabilize the bivalent and monovalent states involved in catalysis. The Co(I) species shows some electronic density spreading over one of the phenolate rings, reinforcing this idea. As these overpotentials and TONs are encouraging in terms of substituents effect for proton reduction, they point out to the possibility of incorporating stronger electron-withdrawing nitro and sulfonic groups to the ligand framework as a means to optimize catalysis. This work is currently under development in our labs.

Conclusions

In this study we investigated the effect of phenolate substituents on the redox and electronic processes of a series of cobalt(III) complexes. These complexes showed the expected Co(III)/Co(II) couple along with multiple ligand-centered redox processes, and the nature of the substituent modulates the potentials by which ligand-based reduction takes place. The visible region of the spectrum dominated by phenolate-to-cobalt(III) and phenolate-to-phenyleneimine charge transfer bands. Upon reduction of the metal center, the LMCT disappears, evidencing the LLCT. The chloro-substituted complex showed promising electron accepting ability. Kinetic plots for chemical reduction favored a relative order as –Cl > –Br > –I > –*t*-Bu. The chloro and *t*-butyl substituted species also showed potential as catalysts for proton reduction in acidic media. Again the chloro-substituted species yielded lower overpotentials than its *t*-Bu counterpart. These overpotentials are considerably negative, therefore, limiting practical use of this framework for efficient proton reduction. Nonetheless they support the notion that incorporation of strong electron-withdrawing groups to the ligand framework may lead to optimized catalytic properties. These efforts are currently under development in our labs.

Materials, methods and synthetic procedures.

General. All reagents and solvents were used as received from commercial sources. Infrared spectra were recorded from 4000 to 650 cm^{-1} as KBr pellets on a Bruker Tensor 27 FTIR spectrophotometer. ^{1}H-NMR spectroscopy was carried out within a Mercury FT-NMR 400 MHz setup using $CDCl_3$ or d^6-DMSO as solvents, at 25 °C. ESI-(+) mass spectrometry were measured in a triple quadrupole Micromass Quattro LC equipment where experimental mass patterns were fitted with theoretical isotopic distribution. Elemental analysis (C, H, and N) determinations were performed using Exeter analytical CHN analyzer by Midwest Microlab: Indianapolis, Indiana. UV–visible spectra were obtained at room temperature using a Varian Cary 50 spectrophotometer operating in the range of 200 to 1000 nm with quartz cells. Values of ε are given in M^{-1} cm^{-1}. All the spectra were recorded in acetonitrile, dichloromethane and dimethylformamide (HPLC-grade) solutions (for CV, UV-Visible) and in CH_3CN–H_2O (90 : 10% v/v) at pH 3.0 with final [complex] = 1.8×10^{-4} M (for chemical reduction).

Electrochemistry and spectroelectrochemistry. The electrochemical behavior of **1–4** was investigated with a BAS 50W potentiostat/galvanostat. Cyclic voltammograms were obtained at room temperature in acetonitrile, dichloromethane or *N*,*N*′-dimethylformamide solutions containing 0.1 M of *n*-Bu_4NPF_6 as supporting electrolyte under argon atmosphere. The electrochemical cell employed was comprised of three electrodes: glassy-carbon (working), platinum wire (auxiliary) and Ag/AgCl (reference). The ferrocene/ferrocenium redox couple Fc/Fc^+ (E° = 400 mV *vs.* NHE)[20] was used as the internal standard. Peak to peak potential separations ($\Delta E_p = |E_{p,c} - E_{p,a}|$) and $|i_{pa}/i_{pc}|$ values were measured to evaluate the reversibility of the redox processes. Spectroelectrostatic measurements were carried out in a optically transparent thin-layer cell (*ca.* 0.1 mm) constructed according to a procedure described as follows: a flat platinum wire in a "u" shape was sandwiched between two glass slides where the inner parts were coated with indium-tin oxide (ITO) (8–12 Ω sq^{-1}). The flat wire acted as the working electrode and extended outside of the slides for electrical contact. The solutions were prepared and degassed under an inert atmosphere (argon) and introduced into the cell through a capillary action. The working electrode was located within 4–6 mm of the cell bottom to minimize ohmic potential (iR) drop. All potentials were measured *vs.* a Ag/AgCl reference electrode and a second platinum wire (counter). Potentials were applied to the cell by a BAS 50W potentiostat/galvanostat, and the spectra were collected with a Varian Cary 50 apparatus at the room temperature within a typical time interval of 30 s until the equilibrium between oxidized/reduced species was achieved.

X-ray structural determination. Diffraction data for **1** and **2** were measured on a Bruker X8 APEX-II kappa geometry diffractometer with Mo radiation and a graphite monochromator and are summarized in Table 5. Frames were collected at 100 K with the detector at 40 mm and 0.3 degrees between each frame and were recorded for 10 s. APEX-II[21] and SHELX[22] software were used in the collection and refinement of the models. Crystals of **1** (CCDC # 1012180) appeared as dark needles. A total of 106 022 reflections were measured, yielding 7148 unique data (R_{int} = 0.074). Hydrogen atoms were placed in calculated positions. These neutral molecules crystallized without ions, solvent or appreciable disorder. Crystals of **2** (CCDC # 1012179) were dark rods. A total of 58 214 reflections were counted, which averaged to 7895 independent data (R_{int} = 0.089). Hydrogen atoms were placed at calculated positions. The solvate molecules occupied sites of symmetry and this did not refine without disorder in the space group *C*2/*c*. The PLATON program SQUEEZE[23] was utilized to include the solvate electrons resulting in an empirical formula of **1** complex: 1 dichloromethane molecule.

Computational methods. Electronic structure calculations were carried out with the Gaussian 09 suite of programs[24]

Table 5 Crystal Data for the complexes **1** and **2**

	1	**2**
Empirical formula	$C_{28}H_{19}Cl_6CoN_2O_4$	$C_{29}H_{21}Br_6Cl_2CoN_2O_4$
Formula weight	719.08	1070.77
Temperature (K)	100(2)	100(2)
Wavelength (Å)	0.71073	0.71073
Crystal system, space group	Monoclinic, *C*2/*c*	Monoclinic, *C*2/*c*
a (Å)	22.0260(10)	28.251(3)
b (Å)	12.9174(6)	13.5819(10)
c (Å)	22.6310(12)	22.091(2)
α (°)	90	90
β (°)	116.109(3)	125.407(7)
γ (°)	90	90
Volume (Å^3)	5781.9(5)	6908.9(10)
Z	8	8
Calculated density (Mg m^{-3})	1.652	2.059
Absorption coefficient (mm^{-1})	1.187	7.629
F (000)	2896	4096
R(*F*) (%)	4.39	8.22
$R_w(F)$ (%)	6.70	11.29

$R(F) = \sum||F_o| - |F_c||/|F_o|$; $R_w(F) = [\sum w(F_o^2 - F_c^2)^2/\sum w(F_o^2)^2]^{1/2}$ for $I > 2\sigma(I)$.

using Density Functional Theory (DFT). The B3PW91/6–31G(d) level of theory[25] was employed throughout. Geometries were fully optimized without symmetry constraints, and stationary points were verified *via* frequency analysis. Solvent effects in dichloromethane and or acetonitrile were estimated using the built-in default settings of the IEF-PCM polarizable continuum model.[26] Cartesian coordinates of all optimized structures are provided as ESI.† Vertical electronic excitation energies and intensities were calculated using time-dependent density functional theory (TD-DFT).[27] Molecular orbitals were plotted with GaussView and UV-visible spectral plots were prepared using SWizard with a full width at half-height of 2000 cm^{-1}. All optimized geometries agreed well with the crystallographic data available for all relevant structures.

Chemical reductions. These experiments were performed in CH_3CN–H_2O (90 : 10% v/v) upon ascorbic acid (reductant) for complexes **1–4** were evaluated spectrophotometrically on a Varian Cary 50 spectrophotometer, at their λ_{max}, respectively by the disappearance/decrease of their ligand-to-metal charge transfer (LMCT) at room temperature. The absorption values were converted into concentration using their absorptivity molar coefficient values (ε, M^{-1} cm^{-1}). All reactions were monitored throughout the time until the absorbance at each λ_{max} value was constant. Reactions were performed using the following conditions: In a 4 mL cuvette (1 cm optical path) were added 2700 μL of a freshly prepared and degassed acetonitrile solution of the complex ($[C]_{final}$ 1.80 × 10^{-4} M), and the reaction was initiated by the addition 300 μL of a aqueous ascorbic acid (pH ∼ 3.0 adjusted with HNO_3; $[AA]_{final}$ = 1.80 × 10^{-2} M). The concentration of the complexes **1–4** towards the elapsed time were plotted and fitted using a typical first order exponential decaying equation $[C] = [C]_0 \times e^{kt}$ and linearized using the first order rate law $\ln[C] = -kt + \ln[C]_0$ where [C] is concentration at a given time (M); $[C]_0$ is the initial concentration (M), *k* is the rate constant (s^{-1}) and *t* is the time (s). The half-lives for the compounds **1–4** were calculated using the expression $t_{1/2} = \ln 2/k$ where $t_{1/2}$ is the half-life and *k* is the rate constant (s^{-1}).

Catalytic activity. Proton reduction electrocatalysis was tested for **1** and **4** *via* cyclic voltammetry in presence of acetic acid (HOAc, pK_a: 22.3 in CH_3CN).[28a] Glassy carbon was used as the working electrode, platinum wire as the auxiliary electrode (15 cm length, from which 13 cm coiled and submerse in solution), and Ag/AgCl as the reference electrode, with tetra-butyl ammonium hexafluorophosphate ($TBAPF_6$) as supporting electrolyte. Overpotentials (η) were calculated from the observed changes in cyclic voltammogram followed by subtracting the thermodynamic standard potential for H^+/H_2 in CH_3CN in the presence of HOAc (after considering the homoconjugation effect[28]) from the experimental half-wave potential for the catalytic peak in the presence of particular amount of HOAc. To determine the amount of hydrogen release, bulk electrolysis has been done in a custom-made air-tight H-type cell using a mercury-pool as working electrode, Ag/AgCl as reference, both in the main chamber. A coiled Pt wire was used as the auxiliary electrode isolated on another compartment by a frit. $TBAPF_6$ was used as the supporting electrolyte. The main chamber was filled with an electrolyte solution and a proton source ($TBAPF_6$: 1.56 g; HOAc: 0.24 g [4 mmol], 20 mL MeCN), whereas the smaller compartment was filled with electrolyte solution ($TBAPF_6$: 0.39 g; 5 mL MeCN). The applied potential for bulk electrolysis is measured against Ag/AgCl and potentials are converted against Fc/Fc^+ upon subtracting the electrochemical potential of Fc/Fc^+ from the applied potential *versus* Ag/AgCl in similar condition. In a typical test, the cell was purged with N_2 gas for 20 min followed by sampling of the head space gas (100μl) to ensure an O_2 free environment in the gas-chromatograph. The GC is a Gow-Mac 400 equipped with a thermal conductivity detector and a 8′ × 1/8″ long 5 Å molecular sieve column operating at 60 °C used with N_2 as the carrier gas. The calibration was carried out with hydrogen (H_2) gas (Hydrogen GC grade 99.99 + %, Scotty analyzed gases, Sigma Aldrich). The solution (no catalyst) was electrolyzed for three hours at −1.8 $V_{Ag/AgCl}$ (−2.2 V_{Fc/Fc^+}) and the head space gas was injected into the GC to record the amount of dihydrogen generated. Then the cell was purged with N_2 gas for another 20 min followed by injection of the catalyst (0.04 mmol) dissolved in MeCN. Bulk electrolysis was conducted for three hours at $-1.8V_{Ag/AgCl}$ (−2.2 V_{Fc/Fc^+}) and the head space gas (100 μL) was injected to the GC instrument. The amount of dihydrogen produced was measured. The turnover number was calculated after background subtraction as the ratio between moles of dihydrogen produced over moles of catalyst used. Faradic efficiency was calculated from GC measurements.

Synthetic procedures.

The 2,4-substituted chloromethylphenols (pendant arms) where –R can be Cl or Br were synthesized under similar

conditions (*vide infra*). The precursor 2-(chloromethyl)-4,6-diiodo-phenol, 2-(chloromethyl)-4,6-di-*tert*-butyl-phenol, and the ligand 6,6′-(((2-((3,5-di-*tert*-butyl-2-hydroxybenzyl)amino)-phenyl)azanediyl)bis(methylene)bis(2,4-di-*tert*-butyl-phenol) ($\mathbf{H_3L^{tBu}}$) were synthesized according methods already described in the literature.[7c,8]

The precursor 2,4-substituted-hydroxymethylphenols. A 70 mL methanol solution of the 3,5-di-substituted-2-hydroxybenzaldehyde (25.0 mmol) was reduced by $NaBH_4$ (60 mmol) at 0 °C overnight. Then, the solvent was removed under reduced pressure and the residual white solid was dissolved in water and the pH was adjusted to ~5.0 with 2.0 M HCl. The product was extracted from water using dichloromethane and dried over anhydrous Na_2SO_4. The solution was filtered and the solvent was removed by rotary evaporation yielding a white colored solid. The crude products were used with no further purification. 2,4-Dichloro-6-(hydroxymethyl)phenol: Yield: 70%. IR (KBr, cm^{-1}) 3281(s) (OH); 3050(w) (Ar–CH); 2948(w) (alkyl–CH); 1596(w), 1580(w), 1474(s) (Ar–C–C); 1166(m) (C–O). ^{1}H-NMR [400 MHz, $CDCl_3$, 300 K] δ/ppm = 2.259 [s, 1H (aliphatic-OH)]; 4.779 [s, 2H (CH_2)]; 6.654 [s, 1H (aryl–OH)]; 7.129 [s, 1H (aryl)]; 7.289 [s, 1H (aryl)]. 2,4-Dibromo-6-(hydroxymethyl)phenol: Yield: 70%. IR (KBr, cm^{-1}) 3508(m), 3241(m) (OH); 3075(w) (Ar–CH); 2934(w) (alkyl–CH); 1456(s) (Ar–C–C); 1141(s) (C–O). ^{1}H-NMR [400 MHz, $CDCl_3$, 300 K] δ/ppm = 2.632 [s, 1H (aliphatic-OH)]; 4.786 [s, 2H (CH_2)]; 4.8 [s, 1H (aryl–OH)]; 6.921 [s, 1H (aryl)]; 7.590 [s, 1H (aryl)].

The precursor 2,4-substituted-chloromethylphenols. Thionyl chloride (50 mmol) was added to the solution of the previously synthesized alcohols (20 mmol) in 30 mL of dichloromethane. After stirring it overnight, the solvent was removed by rotary evaporation and washed five times with *n*-pentane. The 2,4-disubstituted-6-(chloromethyl)phenols were isolated as a white solid and used with no further purification. 2,4-Dichloro-6-(chloromethyl)phenol: Yield: 94%. IR (KBr, cm^{-1}) 3474(s) (OH); 3081(w) (Ar–CH); 2978(w) (alkyl–CH); 1597 (w), 1580(w), 1469(s) (Ar–C–C); 1161(s) (C–O). ^{1}H-NMR [400 MHz, $CDCl_3$, 300 K] δ/ppm = 4.618 [s, 2H (CH_2)]; 5.775 [s, 1H (OH)]; 7.281 [s, 1H (aryl)]; 7.322 [s, 1H (aryl)]. 2,4-Dibromo-6-(chloromethyl)phenol: Yield: 90%. IR (KBr, cm^{-1}) 3462(s) (OH); 3066(w) (Ar–CH); 2971(w) (alkyl–CH); 1461(s) (Ar–C–C); 1143(s) (C–O). ^{1}H-NMR [400 MHz, $CDCl_3$, 300 K] δ/ppm = 4.618 [s, 2H (CH_2)]; 5.761 [s, 1H (aryl–OH)]; 7.445 [s, 1H (aryl)]; 7.577 [s, 1H (aryl)].

The proligands. Phenylene diamine (2 mmol) was treated with the appropriate 2,4-disubstituted-6-(chloromethyl)-phenol (6.2 mmol) in presence of triethylamine (8 mmol) in 80 mL of dichloromethane for 3 days under reflux to yield a yellow colored solution. The mixture was washed three times with brine solution (3 × 200 mL) to remove excess triethylamine, dried over anhydrous sodium sulfate and the crude product was isolated by solvent rotoevaporation. Unreacted chloride was removed by washing the solid with cold hexane to yield a yellow-colored solid. Upon coordination to the metal these amine proligands are stabilized as imine ligands.[8]

6,6′-(((2-((3,5-Dichloro-2-hydroxybenzyl)amino)phenyl)azanediyl)-bis(methylene)bis(2,4-dichlorophenol) – $H_3L'^{Cl}$. Yield: 75%. IR (KBr, cm^{-1}) 3505(w), 3414(w) (OH); 3263(w) (NH); 3078(w) (Ar–CH); 2983(w) (alkyl–CH); 1599(m), 1467(s) (Ar–C–C); 1165(m) (C–O). ^{1}H-NMR [400 MHz, $CDCl_3$, 300 K] δ/ppm = 4.093 [s, 4H (CH_2)]; 4.263 [s, 2H (CH_2)]; 6.61 [d, 1H (aryl)]; 6.776 [t, 1H (aryl)]; 6.887 [s, 2H (aryl)]; 7.011 [t, 1H (aryl)]; 7.068 [s, 1H (aryl)]; 7.167 [d, 1H (aryl)]; 7.212 [s, 2H (aryl)]; 7.3 [s, 1H (aryl)]. ESI pos. in MeOH: m/z = 630.9670 for $[H_3L_1 + H^+]^+$.

6,6′-(((2-((3,5-Dibromo-2-hydroxybenzyl)amino)phenyl)azanediyl)-bis(methylene)bis(2,4-dibromophenol) – $H_3L'^{Br}$. Yield: 70%. IR (KBr, cm^{-1}) 3490(w) (OH); 3252(w) (NH); 3070(w) (Ar–CH); 2982(w) (alkyl–CH); 1598(m), 1455(s) (Ar–C–C); 1144(m) (C–O). ^{1}H-NMR [400 MHz, $CDCl_3$, 300 K] δ/ppm = 4.096 [s, 4H (CH_2)]; 4.249 [s, 2H (CH_2)]; 6.644 [d, 1H (aryl)]; 6.798 [t, 1H (aryl)]; 7.023 [t, 3H (aryl)]; 7.157 [d, 1H (aryl)]; 7.268 [s, 1H (aryl)]; 7.475 [s, 2H (aryl)]; 7.542 [s, 1H (aryl)] ESI pos. in MeOH: m/z = 894.7 for $[H_3L_2 + H^+]^+$.

6,6′-(((2-((2-Hydroxy-3,5-diiodobenzyl)amino)phenyl)azanediyl)-bis(methylene))bis(2,4-diiodophenol) – $H_3L'^{I}$. Yield: 73%. IR (KBr, cm^{-1}) 3385(w) (OH); 3226(w) (NH); 3061(w) (Ar–CH); 2920(w) (alkyl–CH); 1598(m), 1451(s) (Ar–C–C); 1147(m) (C–O). ^{1}H-NMR [400 MHz, $CDCl_3$, 300 K] δ/ppm = 4.07 [s, 4H (CH_2)]; 4.238 [s, 2H (CH_2)]; 6.733[t, 2H (aryl)]; 6.867 [t, 1H (aryl)]; 7.077 [t, 2H (aryl)]; 7.183 [d, 2H (aryl)]; 7.526 [s, 1H (aryl)]; 7.809 [s, 1H (aryl)]; 7.961 [s, 1H (aryl)] ESI pos. in MeOH: m/z = 1182.582 for $[H_3L_3 + H^+]^+$.

The complexes. Caution: Perchlorate salts are potentially explosive and should be handled in small quantities and with care.

Complexes **1–4** have been synthesized under aerobic conditions using the general procedure described as follows: to a 30 mL solution of ligand in dichloromethane (1 mmol) were added sodium methoxide (0.162 g, 3 mmol) in 30 mL of methanol and the mixture was stirred for 10 minutes. A 20 mL methanol solution of $[Co(H_2O)_6](ClO_4)_2$ (0.365 g, 1 mmol) were added dropwise to the mixture in a period of 5 minutes. After the addition was complete, the solution was refluxed for 4 hours to ensure the completion of reaction and the mixture was concentrated to 10 mL. Slow evaporation of the solvent gives rise to brown colored precipitate which has been collected by vaccum filtration. Further recrystalization form different solvent mixtures give crystalline pure product.

*[$Co^{III}(L^{Cl})$MeOH] (**1**).* Recrystallized from MeOH–di-ethyl ether (1 : 1). Yield. 80%. IR (KBr, cm^{-1}) 3444(w) (OH); 3063(w) (Ar–CH); 2950(w) (alkyl–CH); 1612(s), 1450(s) (Ar–C–C); 1584 (m) (C═N); 1177(m) (C–O); No ClO_4^-. ^{1}H-NMR [400 MHz, d^6-DMSO, 300 K] δ/ppm = 3.150 [d, 3H (CH_3)]; 3.967 [d, 2H (CH_2)]; 4.083 [q, 1H (OH)]; 4.767 [d, 2H (CH_2)]; 6.734 [s, 2H (aryl)]; 6.820 [s, 2H (aryl)]; 7.138 [t, 1H (aryl)]; 7.300 [t, 1H (aryl)]; 7.552 [s, 1H (aryl)]; 7.645 [s, 1H (aryl)]; 7.686 [d, 1H (aryl)]; 7.955 [s, 1H (N═CH)]; 8.056 [d, 1H (aryl)]. ESI pos. in MeOH: m/z = 684.8624 for $[Co^{III}(L'^{Cl}) + H^+]^+$. Anal. Calcd for $C_{28}H_{19}Cl_6CoN_2O_4$: C, 46.77; H, 2.66; N, 3.90. Found: C, 46.46; H, 2.64; N, 4.00.

[$Co^{III}(L^{Br})$MeOH] (2). Recrystallized from MeOH–DCM (1 : 1). Yield. 85%. IR (KBr, cm^{-1}) 3263(w) (OH); 3050(w) (Ar–CH); 2945(w) (alkyl–CH); 1612(m), 1442(s) (Ar–C–C); 1584(m) (C═N); 1157(m) (C–O); No ClO_4^-. ^{1}H-NMR [400 MHz, d^6-DMSO, 300 K] δ/ppm = 3.149 [d, 3H (CH_3)]; 3.977 [d, 2H (CH_2)]; 4.077 [q, 1H (OH)]; 4.8 [d, 2H (CH_2)]; 6.877 [s, 2H aryl)]; 7.032 [s, 2H (aryl)]; 7.145 [t, 1H (aryl)]; 7.295 [t, 1H (aryl)]; 7.693 [d, 1H (aryl)]; 7.724 [s, 1H (aryl)]; 7.843 [s, 1H (aryl)]; 7.981 [s, 1H (N═CH)]; 8.054 [d, 1H (aryl)]. ESI pos. in MeOH: m/z = 954.5676 for [$Co^{III}(L'^{Br})$ + Li^+]$^+$. Anal. Calcd for $C_{28}H_{19}Br_6CoN_2O_4$: C, 34.11; H, 1.94; N, 2.84. Found: C, 33.60; H, 1.81; N, 2.95.

[$Co^{III}(L^{I})$MeOH] (3). **^{i}PrOH** Recrystallized from DCM–isopropanol (1 : 1). Yield. 90%. IR (KBr, cm^{-1}) 3443(w) (OH); 3047(w) (Ar–CH); 2925(w) (alkyl–CH); 1610(m), 1427(s) (Ar–C–C); 1581 (m) (C═N); 1150(m) (C–O); No ClO_4^-. ^{1}H-NMR [400 MHz, d^6-DMSO, 300 K] δ/ppm = 3.147 [d, 3H (CH_3)]; 3.945 [d, 2H (CH_2)]; 4.01 [q, 1H (OH)]; 4.808 [d, 2H (CH_2)]; 6.978 [s, 2H aryl)]; 7.065 [t, 1H (aryl)]; 7.116 [t, 1H (aryl)]; 7.271 [s, 2H aryl)]; 7.718 [d, 1H (aryl)]; 7.843 [d, 1H (aryl)]; 7.945 [s, 1H (N═CH)]; 8.044 [s, 2H (aryl)]. ESI pos. in MeOH: m/z = 1242.4844 for [$Co^{III}(L'^{I})$ + Li^+]$^+$. Anal. Calcd for $C_{31}H_{27}I_6CoN_2O_5$: C, 28.04; H, 2.05; N, 2.11 Found: C, 28.55; H, 1.55; N, 2.52.

[$Co^{III}(L^{t\text{-}Bu}$MeOH].[8] *(4).* Recrystallized from MeOH–DCM. ^{1}H-NMR [400 MHz, d^6-DMSO, 300 K] δ/ppm = 0.86 [s, 18H (*t*-butyl)]; 1.00 [s, 18H (*t*-butyl)]; 1.24 [s, 9H (*t*-butyl)]; 1.62 [s, 9H (*t*-butyl)]; 3.145 [d, 3H (CH_3)]; 3.855 [d, 2H (CH_2)]; 4.085 [q, 1H (OH)]; 4.865 [d, 2H (CH_2)]; 6.46 [s, 2H (aryl)]; 6.53 [s, 2H (aryl)]; 6.88 [t, 1H (aryl)]; 7.08 [t, 1H (aryl)]; 7.10 [s, 1H (aryl)]; 7.28 [s, 1H (aryl)]; 7.53 [s, 1H (N═CH)]; 7.645 [d, 1H (aryl)]; 8.035 [d, 1H (aryl)].

Acknowledgements

This material is based upon work supported by the U.S. Department of Energy, Office of Science, Office of Basic Energy Sciences under award number DE-SC0001907 to C. N. V. and H. B. S., including financial support for D. B. (synthesis, characterizations, catalysis), M. M. A. (DFT calculations), and F. R. X. (spectroelectrochemistry, kinetics). Equipment use at the WSU-Lumigen Instrument Center and computer time allocated at the WSU-Grid System for DFT calculations is also acknowledged.

References

1 (*a*) P. D. Tran, V. Artero and M. Fontecave, *Energy Environ. Sci.*, 2010, **3**, 727; (*b*) M. G. Walter, E. L. Warren, J. R. McKone, S. W. Boettcher, Q. Mi, E. A. Santori and N. S. Lewis, *Chem. Rev.*, 2010, **110**, 6446; (*c*) T. R. Cook, D. K. Dogutan, S. Y. Reece, Y. Surendranath, T. S. Teets and D. G. Nocera, *Chem. Rev.*, 2010, **110**, 6474; (*d*) A. J. Esswein and D. G. Nocera, *Chem. Rev.*, 2007, **107**, 4022; (*e*) N. S. Lewis and D. G. Nocera, *Proc. Natl. Acad. Sci. U. S. A.*, 2006, **103**, 15729; (*f*) J. A. Turner, *Science*, 2004, **305**, 972.

2 (*a*) W. R. McNamara, Z. Han, C. J. Yin, W. W. Brennessel, P. L. Holland and R. Eisenberg, *Proc. Natl. Acad. Sci. U. S. A.*, 2012, **109**, 15594; (*b*) M. T. D. Nguyen, M. F. Charlot and A. Aukauloo, *J. Phys. Chem. A*, 2011, **115**, 911; (*c*) B. D. Stubbert, J. C. Peters and H. B. Gray, *J. Am. Chem. Soc.*, 2011, **133**, 18070.

3 (*a*) S. C. Marinescu, J. R. Winkler and H. B. Gray, *Proc. Natl. Acad. Sci. U. S. A.*, 2012, **109**, 15127; (*b*) J. T. Muckermann and E. Fujita, *Chem. Commun.*, 2011, **47**, 12456; (*c*) B. H. Solis and S. Hammes-Schiffer, *Inorg. Chem.*, 2011, **50**, 11252.

4 (*a*) C. C. McCrory, L. C. Uyeda and J. C. Peters, *J. Am. Chem. Soc.*, 2012, **134**, 3164; (*b*) W. M. Singh, T. Baine, S. Kudo, S. Tian, X. A. N. Ma, H. Zhou, N. J. DeYonker, T. C. Pham, J. C. Bollinger, D. L. Baker, B. Yan, C. E. Webster and X. Zhao, *Angew. Chem., Int. Ed.*, 2012, **51**, 5941; (*c*) W. R. McNamara, Z. Han, C. J. Yin, W. W. Brennessel, P. L. Holland and R. Eisenberg, *Proc. Natl. Acad. Sci. U. S. A.*, 2012, **109**, 15594; (*d*) L. M. Utschig, S. C. Silver, K. L. Mulfort and D. M. Tiede, *J. Am. Chem. Soc.*, 2011, **133**, 16334; (*e*) T. M. McCormick, Z. Han, D. J. Weinberg, W. W. Brennessel, P. L. Holland and R. Eisenberg, *Inorg. Chem.*, 2011, **50**, 10660; (*f*) C. F. Leung, Y. Z. Chen, H. Q. Yu, S. M. Yiu, C. C. Ko and T. C. Lau, *Int. J. Hydrogen Energy*, 2011, **36**, 11640; (*g*) Y. Sun, J. P. Bigi, N. A. Piro, M. L. Tang, J. R. Long and C. J. Chang, *J. Am. Chem. Soc.*, 2011, **133**, 9212; (*h*) B. Probost, A. Rodenberg, M. Guttentag, P. Hamm and R. Alberto, *Inorg. Chem.*, 2010, **49**, 6453; (*i*) P. A. Jacques, V. Artero, J. Pecaut and M. Fontecave, *Proc. Natl. Acad. Sci. U. S. A.*, 2009, **106**, 20627; (*j*) P. Du, J. Schneider, G. Luo, W. W. Brennessel and R. Eisenberg, *Inorg. Chem.*, 2009, **48**, 4952; (*k*) C. Li, M. Wang, J. Pan, P. Zhang, R. Zhang and L. Sun, *J. Organomet. Chem.*, 2009, **694**, 2814; (*l*) A. Fihri, V. Artero, A. Pereira and M. Fontecave, *Dalton Trans.*, 2008, 5567; (*m*) C.-F. Leung, S.-M. Ng, C.-C. Ko, W.-L. Man, J. Wu, L. Chen and T.-C. Lau, *Energy Environ. Sci.*, 2012, **5**, 7903; (*n*) S. Varma, C. E. Castillo, T. Stoll, J. Fortage, A. G. Blackman, F. Moltan, A. Deronzier and M.-N. Collomb, *Phys. Chem. Chem. Phys.*, 2013, **15**, 17544; (*o*) L. Tong, R. Zong and R. P. Thummel, *J. Am. Chem. Soc.*, 2014, **136**, 4881; (*p*) C. Bachmann, B. Probst, M. Guttentag and R. Alberto, *Chem. Commun.*, 2014, **50**, 6737; (*q*) M. Natali, A. Luisa, E. Lengo and F. Scandola, *Chem. Commun.*, 2014, **50**, 1842.

5 (*a*) R. M. Thomas, P. C. B. Widger, S. M. Ahmed, R. C. Jeske, W. Hirahata, E. B. Lobkovsky and G. W. Coates, *J. Am. Chem. Soc.*, 2010, **132**, 16520; (*b*) E. N. Jacobsen, *Acc. Chem. Res.*, 2000, **33**, 421.

6 (*a*) L. Chiang, L. E. N. Allan, J. Alcantara, M. C. P. Wang, T. Storr and M. P. Shaver, *Dalton Trans.*, 2014, **43**, 4295; (*b*) B. Solis, Y. Yu and S. Hammes-Schiffer, *Inorg. Chem.*, 2013, **52**, 6994; (*c*) A. Kochem, F. Thomas, O. Jarjayes,

G. Gellon, C. Philouze, T. Weyhermüller, F. Neese and M. Van Gastel, *Inorg. Chem.*, 2013, **52**, 14428; (*d*) A. Kochem, H. Kanso, B. Baptiste, H. Arora, C. Philouze, O. Jarjayes, H. Vezin, D. Luneau, M. Orio and F. Thomas, *Inorg. Chem.*, 2012, **51**, 10557.

7 (*a*) F. D. Lesh, R. L. Lord, M. J. Heeg, H. B. Schlegel and C. N. Verani, *Eur. J. Inorg. Chem.*, 2012, 463; (*b*) D. Tomco, F. R. Xavier, M. M. Allard and C. N. Verani, *Inorg. Chim. Acta*, 2012, **393**, 269; (*c*) D. Tomco, S. Schmitt, B. Ksebati, M. J. Heeg, Q. P. Dou and C. N. Verani, *J. Inorg. Biochem.*, 2011, **105**, 1759; (*d*) R. Shakya, S. S. Hindo, L. Wu, M. M. Allard, M. J. Heeg, H. P. Hratchian, B. R. McGarvey, S. R. P. D. Rocha and C. N. Verani, *Inorg. Chem.*, 2007, **46**, 9808; (*e*) R. Shakya, C. Imbert, H. P. Hratchian, M. Lanznaster, M. J. Heeg, B. R. McGarvey, M. M. Allard, H. B. Schlegel and C. N. Verani, *Dalton Trans.*, 2006, 2517.

8 M. M. Allard, F. R. Xavier, M. J. Heeg, H. B. Schlegel and C. N. Verani, *Eur. J. Inorg. Chem.*, 2012, 4622.

9 (*a*) M. Lanznaster, M. J. Heeg, G. T. Yee, B. R. McGarvey and C. N. Verani, *Inorg. Chem.*, 2007, **46**, 72; (*b*) M. M. Allard, J. A. Sonk, M. J. Heeg, B. R. McGarvey, H. B. Schlegel and C. N. Verani, *Angew. Chem., Int. Ed.*, 2012, **51**, 3178; (*c*) L. D. Wickramasinghe, M. M. Perera, L. Li, G. Mao, Z. Zhou and C. N. Verani, *Angew. Chem., Int. Ed.*, 2013, **52**, 13346.

10 (*a*) L. J. Farrugia, ORTEP for windows, *J. Appl. Crystallogr.*, 1997, **30**, 565; (*b*) L. Zsolnai, *ZORTEP: an interactive ortep program*, University of Heidelberg, Germany, 1997.

11 G. M. Zats, H. Arora, R. Lavi, D. Yufit and L. Benisvy, *Dalton Trans.*, 2011, **40**, 10889.

12 A. Sokolowski, B. Adam, T. Weyhermuller, A. Kikuchi, K. Hildenbrand, R. Schnepf, P. Hildebrandt, E. Bill and K. Wieghardt, *Inorg. Chem.*, 1997, **36**, 3702.

13 (*a*) A. A. Khandar, B. Shaabani, F. Belaj and A. Bakhtiari, *Inorg. Chim. Acta*, 2007, **360**, 3255; (*b*) A. H. Sarvestani and S. J. Mohebbi, *Chem. Res.*, 2006, 257; (*c*) M. S. Shongwe, S. K. M. Al-Hatmi, H. M. Marques, R. Smith, R. Nukada and M. Mikuriya, *J. Chem. Soc., Dalton Trans.*, 2002, 4064; (*d*) D. G. McCollum, G. P. A. Yap, A. L. Rheingold and B. Bosnich, *J. Am. Chem. Soc.*, 1996, **118**, 1365.

14 M. I. Davis, A. M. Orville, F. Neese, J. M. Zaleski, J. D. Lipscomb and E. I. Solomon, *J. Am. Chem. Soc.*, 2002, **124**, 602.

15 (*a*) S. Koyuncu, I. Kaya, F. B. Koyuncu and E. Ozdemir, *Synth. Met.*, 2009, **159**, 1034; (*b*) S. A. M. Refaey, A. A. Hassan and H. S. Shehata, *Int. J. Electrochem. Sci.*, 2008, **3**, 325.

16 A. Bottcher, T. Takeuchi, K. I. Hardcastle, T. J. Meade, H. B. Gray, D. Cwikel, M. Kapon and Z. Dori, *Inorg. Chem.*, 1997, **36**, 2498.

17 (*a*) P. D. Metelski, Y. Fu, K. Khan and T. W. Swaddle, *Inorg. Chem.*, 1999, **38**, 3103; (*b*) J. F. Endicott and T. Ramasami, *J. Phys. Chem.*, 1986, **90**, 3740.

18 L. Benisvy, E. Bill, A. J. Blake, D. Collison, E. S. Davies, C. D. Garner, C. I. Guindy, E. J. L. McInnes, G. McArdle, J. McMaster, C. Wilson and J. Wolowska, *Dalton Trans.*, 2004, 3647.

19 A. Neves, W. Herrmann and K. Wieghardt, *Inorg. Chem.*, 1984, **23**, 3435.

20 R. Gagne, C. Koval and G. Licenski, *Inorg. Chem.*, 1980, **19**, 2854.

21 *APEX II collection and processing programs are distributed by the manufacturer*, Bruker AXS Inc., Madison, WI, USA, 2009.

22 G. M. Sheldrick, *Acta Crystallogr., Sect. A: Fundam. Crystallogr.*, 2008, **64**, 112.

23 A. L. Spek, *J. Appl. Crystallogr.*, 2003, **36**, 7.

24 M. J. Frisch, G. W. Trucks, H. B. Schlegel, G. E. Scuseria, M. A. Robb, J. R. Cheeseman, G. Scalmani, V. Barone, B. Mennucci, G. A. Petersson, H. Nakatsuji, M. Caricato, X. Li, H. P. Hratchian, A. F. Izmaylov, J. Bloino, G. Zheng, J. L. Sonnenberg, M. Hada, M. Ehara, K. Toyota, R. Fukuda, J. Hasegawa, M. Ishida, T. Nakajima, Y. Honda, O. Kitao, H. Nakai, T. Vreven, J. A. Montgomery, J. E. Peralta, F. Ogliaro, M. Bearpark, J. Heyd, J. E. Brothers, K. N. Kudin, V. N. Staroverov, R. Kobayashi, J. Normand, K. Raghavachari, A. Rendell, J. C. Burant, S. S. Iyengar, J. Tomasi, M. Cossi, N. Rega, J. M. Millam, M. Klene, J. E. Knox, J. B. Cross, V. Bakken, C. Adamo, J. Jaramillo, R. Gomperts, R. E. Stratmann, O. Yazyev, A. J. Austin, R. Cammi, C. Pomelli, J. W. Ochterski, R. L. Martin, K. Morokuma, V. G. Zakrzewski, G. A. Voth, P. Salvador, J. J. Dannenberg, S. Dapprich, P. V. Parandekar, N. J. Mayhall, A. D. Daniels, O. Farkas, J. B. Foresman, J. V. Ortiz, J. Cioslowski and D. J. Fox, *Gaussian G09*, Wallingford, CT, 2009.

25 (*a*) A. D. Becke, *J. Chem. Phys.*, 1993, **98**, 5648; (*b*) J. P. Perdew, *Phys. Rev. B: Condens. Matter*, 1986, **33**, 8822; (*c*) J. P. Perdew, K. Burke and Y. Wang, *Phys. Rev.*, 1996, **54**, 16533.

26 (*a*) S. Miertus, E. Scrocco and J. Tomasi, *Chem. Phys.*, 1981, **55**, 117; (*b*) J. Tomasi, B. Mennucci and R. Cammi, *Chem. Rev.*, 2005, **105**, 2999; (*c*) G. Scalmani, M. J. Frisch, B. Mennucci, J. Tomasi, R. Cammi and V. Barone, *J. Chem. Phys.*, 2006, **124**, 9410; (*d*) G. Scalmani and M. J. Frisch, *J. Chem. Phys.*, 2010, **132**, 114110; (*e*) J. Tomasi, B. Mennucci and R. Cammi, *Chem. Rev.*, 2005, **105**, 2999.

27 (*a*) E. Runge and E. K. U. Gross, *Phys. Rev. Lett.*, 1984, 52; (*b*) R. E. Stratmann, G. E. Scuseria and M. J. Frisch, *J. Chem. Phys.*, 1998, **109**, 8218.

28 (*a*) V. Fourmond, P. A. Jacques, M. Fontecave and V. Artero, *Inorg. Chem.*, 2010, **49**, 10338; (*b*) J. A. S. Roberts and R. M. Bullock, *Inorg. Chem.*, 2013, **52**, 3823; (*c*) A. M. Appel and M. L. Helm, *ACS Catal.*, 2014, **4**, 630.

